OPTIMIZATION OF THERMAL PERFORMANCE OF A DOUBLE-TUBE HEAT EXCHANGER WITH DISCONTINUOUS HIGH-LOW DOUBLE-HELICAL FINS

Kan Cao*[*1], Wannian Ma[1], Dan Ma[2], Shaofei Huang[1], Lei Li[1], Jiaxing Liang[1], and Zhiwei Kang[1]

[1]School of Smart Energy and Environment, Zhongyuan University of Technology, Zhengzhou, 450007, China

[2]Henan Yicheng Holdings Co., Ltd. Zhengzhou, 450000, China

[*]Corresponding author: caokan96@163.com

In industrial waste-heat recovery, double-tube heat exchangers are widely used owing to their structural adaptability and operational reliability. To enhance thermal performance, this study proposes a discontinuous high–low double helical fin double-tube heat exchanger and numerically investigates the effects of fin discontinuity distance, low-fin height, and helix angle on shell-side flow and heat transfer. The results indicate that periodic axial interruptions combined with alternating fin heights intensify turbulence and promote fluid mixing, thereby enhancing heat transfer. Response Surface Methodology is used to optimize the structural parameters, and the results show that the helix angle is the dominant factor, with a notable interaction with the fin discontinuity distance. Under the optimal conditions of a fin discontinuity distance of 142.5 mm, a low-fin height of 12.1 mm, and a helix angle of 59.3°, the optimized configuration increases the Nusselt number by 28.25%, reduces the friction factor by 9.68%, and improves the performance evaluation criterion by 38% compared with a conventional single helical fin configuration. These findings provide quantitative guidance for the design of high-efficiency double-tube heat exchangers.

Key words: *Double-tube heat exchanger; Discontinuous high-low double-helical fins; Heat transfer enhancement; Response Surface Methodology; Field synergy*

1. Introduction

Heat exchangers are fundamental devices for thermal energy transfer and are widely employed in industries such as chemical processing, petroleum refining, refrigeration, aerospace thermal control, and waste-heat recovery [1, 2]. Among these configurations, the double-tube heat exchanger (DTHE) is extensively used in engineering applications owing to its simple structure, operational reliability, and broad applicability [3-5]. Existing strategies for enhancing shell-side heat transfer in DTHEs include modifications of the inner-tube geometry, the adoption of composite structural designs, and the application of nanofluids. In addition, alternative

waste-heat recovery concepts, such as heat-pipe and pulsating heat-pipe devices, have been investigated [6-8]. Meanwhile, active enhancement methods, including ultrasonic vibration, have been explored to intensify fluid mixing and disrupt thermal boundary layers in heat exchangers [9-12]. In recent years, fin structures applied to the inner-tube surface have attracted increasing attention because they offer a cost-effective means of improving heat transfer, indicating considerable potential for enhancing the performance of DTHEs.

Modifying the inner-tube geometry in a DTHE can effectively enhance heat transfer performance. Liu et al. [13] experimentally compared a self-supporting twisted elliptical tube bundle with a conventional circular tube bundle in an oil cooler under shell-side conditions, and found that the elliptical bundle significantly improved heat transfer efficiency while reducing flow resistance at low Reynolds numbers (*Re*). Barati et al. [14] combined experiments and numerical simulations to investigate alternating flat tubes, reporting that an optimized alternating angle increased overall thermal performance by up to 54% relative to circular pipes. Al-Obaidi et al. [15] developed a three-dimensional numerical model to examine the influence of corrugation geometry on flow and heat transfer; validation against experimental data showed that, for *Re* = 4,000–12,000, ring spacing, corrugation arc angle, and circumferential distribution play critical roles in governing performance. Alhamid et al. [16] systematically analyzed circular-arc recessed corrugated tubes and reported a peak performance evaluation at an arc diameter of 0.5 mm and *Re* = 1,500. Wu et al. [17] modeled a DTHE with inner and outer corrugated spiral tubes, showing that optimized corrugation depth and pitch enhanced heat transfer, increasing the Nusselt number (*Nu*) by 40.3%–97.3% and improving performance evaluation criterion (*PEC*) by 12.8%–65.9%. Similarly, passive enhancement concepts such as twisted-tube inserts and helical or coiled tube configurations have been investigated to improve heat transfer by intensifying secondary flow and promoting fluid mixing [18-23].

Composite structural designs have also been shown to improve DTHE performance. Insert-based approaches, including twisted-tape and wire-coil configurations, have been reported to enhance the overall thermal performance of double-pipe heat exchangers [24, 25]. Chaurasia and Sarviya [26] found that double-twist tape inserts yielded higher *Nu* and pressure drops, but achieved superior overall thermal performance compared with single-twist inserts. Hussein et al. [27] reported that semi-circular perforated baffles on the annulus side increased the average overall heat transfer coefficient by 80.6% at an optimal perforation diameter of 20 mm, and that the thermal performance factor exceeded unity for all perforated cases. Barzegar et al. [28] showed that rectangular-cut twisted tape (RCT) improves performance relative to conventional twisted tape and no-insert configurations; the thermal-performance factor reached 1.46 at a cut-depth ratio of 0.33 and width ratio of 0.15. For nanofluids, For nanofluids, Demir et al. [29] demonstrated substantial heat transfer enhancement at low nanoparticle concentrations using two-dimensional single-phase simulations, whereas Reddy et al. [30] experimentally investigated a DTHE using a titanium dioxide–water/ethylene glycol hybrid nanofluid combined with wire-coil inserts. At a nanoparticle volume fraction of 0.02%, the heat transfer coefficient and the friction factor (*f*) increased by 10% and 8.73%, respectively, compared with the base fluid; with wire-coil inserts, these increases rose to 13.85% and 10.89%. Recent studies and reviews further indicate that nanofluid type and concentration can enhance convective heat transfer in double-pipe heat exchangers, typically at the expense of increased flow resistance [31-34].

Both straight and helical fin configurations can enhance DTHE performance. Kahalerras and Targui [35] showed that increasing porous-fin height can substantially raise the mean *Nu* at $R_k = 1$. Maakoul et al. [36] proposed the application of segmented longitudinal straight fins in double-tube heat exchangers, resulting in a 31%–48% increase in heat transfer rate at the same pumping power compared with conventional straight fins. Using GA coupled with a discontinuous Galerkin FEM, Iqbal et al. [37, 38] optimized longitudinal fin profiles and achieved up to a 289% increase in the heat transfer coefficient, depending on the characteristic diameter used for tuning. Using field synergy theory, Wang et al. [39] designed a staggered helical fin DTHE that reduced pressure drop by 10%–30% and improved overall efficiency relative to a conventional straight helical fin model. Parinya et al. [40] compared embedded and welded helical fin exchangers on the air side, reporting superior thermal performance for embedded fins due to more reliable fin–tube junctions, whereas welded fins incurred higher pressure losses from slag at the fin roots. Hosseinkhani et al. [41] performed multi-objective optimization on a spiral baffle fin gas-to-gas DTHE for flare-gas recovery and found that reducing fin pitch enhances heat transfer but increases flow resistance; gas-phase radiation raised heat flux with little hydraulic penalty, enabling identification of an optimal trade-off. In this context,, studies on helical fin designs have shown that fin number and arrangement strongly influence the balance between heat transfer enhancement and flow resistance in double-pipe heat exchangers [42, 43].

Previous studies have shown that modifying inner-tube geometry can enhance shell-side heat transfer by increasing flow disturbance; however, such approaches are often accompanied by a substantial rise in flow resistance. Composite enhancement structures can further improve thermal performance, but their practical implementation is frequently limited by excessive pressure drop, increased manufacturing complexity, and reduced structural adaptability. In other enhanced passages, it is also observed that increasing flow disturbance to improve heat transfer simultaneously increases frictional losses and raises fabrication requirements. [44-47].

Helical fins are widely used in DTHEs because they induce swirling flow and enhance convective heat transfer. Nevertheless, most existing helical fin designs employ continuous and uniform fin geometries, which tend to maintain strong swirl throughout the annulus. Consequently, flow resistance may increase markedly, while the ability to regulate local flow structures remains limited, making it difficult to achieve an optimal balance between heat transfer enhancement and pressure drop.

To address this issue, the present study proposes a discontinuous high–low double-helical fin configuration. Periodic flow interruption and fin height variation are introduced to weaken the persistence of the helical boundary layer, thereby enhancing heat transfer while mitigating excessive pressure losses. Shell side flow and heat transfer characteristics are investigated using numerical simulations, and Response Surface Methodology (RSM) is employed to optimize the structural parameters. The results provide quantitative support and design guidance for high efficiency DTHEs.

2. Physical model

Fig. 1(a) presents a schematic of the physical model of the DTHE. As shown in fig. 1(b), the conventional configuration employs a single helical fin, whereas fig. 1(c) illustrates the

effective heat transfer section of the investigated DTHE with discontinuous high–low double-helical fins. In the proposed design, air flows through a helical passage formed by the annular gap between the inner and outer tubes and the spiral fins. The fin thickness is denoted by δ, and the fins are made of copper. The double-helical fins comprise alternating high and low fins: the high fins have a height equal to the annular gap, H = 14 mm, while the low fins have a height of h = 7 mm. The initial low fin height is set to 7 mm, approximately one half of the high fin height, based on previous numerical analyses. At h = 7 mm, shell side disturbance and mixing are sufficiently developed; therefore, this configuration is adopted as the baseline case.

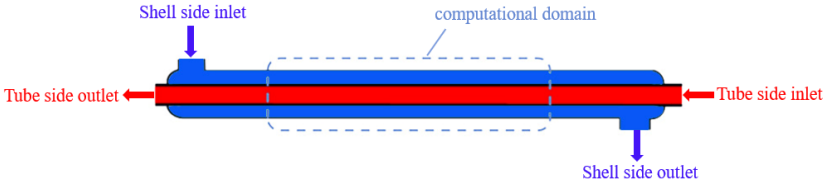

(a) Schematic illustration of the physical model of the DTHE

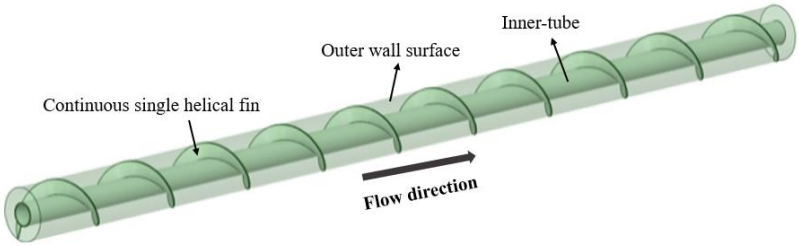

(b) Computational domain of the conventional single helical fin DTHE

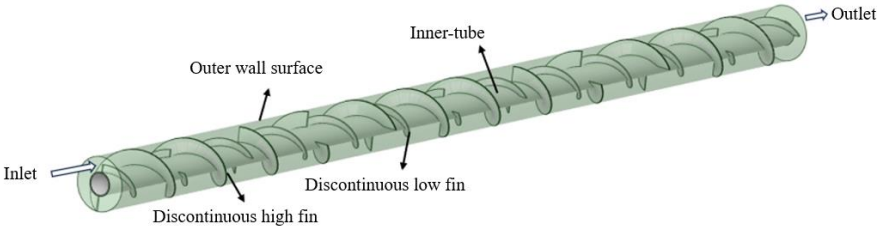

(c) Computational domain of the discontinuous high-low double-helical fins DTHE

Fig. 1. Schematic illustration of the model

Different helix angles correspond to different pitches. As shown in fig. 2(a), the helix angle α is defined as the angle between the helix line and the plane perpendicular to the tube axis. Consider the right triangle ABC, in which the base AB is wrapped into a circle; the length of AB corresponds to the inner-tube circumference (that is, the projected circumference of the helix line), BC represents the pitch S, and AC denotes the developed length of one helix pitch [48]. Accordingly, α can be expressed as follows:

$$\alpha = \arctan \frac{S}{\pi d} \tag{1}$$

Fig. 2(b) presents a schematic of the fin geometric parameters. The discontinuous fin pattern is implemented by dividing the helical fins into discrete blocks. Each fin block extends circumferentially and axially over a prescribed distance S and then terminates; the subsequent block is circumferentially offset by 90°, as illustrated in fig. 2(c). This arrangement preserves an overall double-helical appearance while introducing periodic interruptions that modify the flow path and promote mixing. The detailed geometric parameters and notation are listed in tab.

1. The model dimensions were selected based on commonly used configurations reported in previous DTHE studies, together with general heat exchanger design guidelines, to provide adequate flow passage, avoid excessive blockage, and ensure structural and manufacturing feasibility.

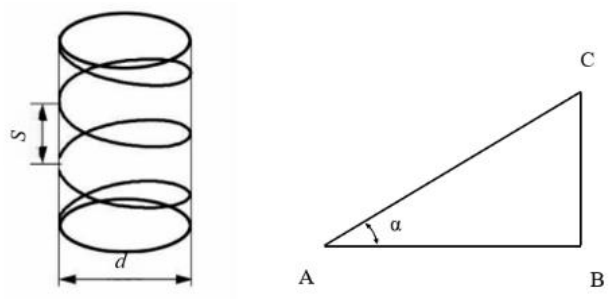

(a) Schematic of the helix angle calculation

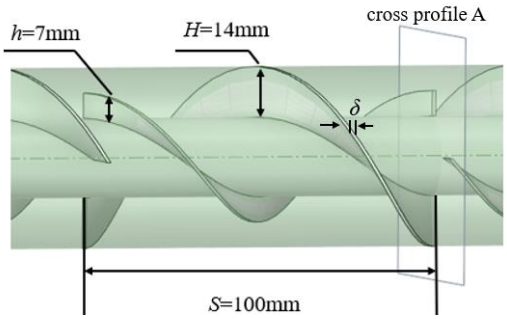

(b) Fin structural parameters

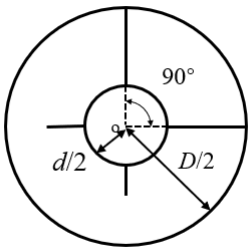

(c) cross-section at section A

Fig. 2. Schematic of model parameters

Tab. 1. Fundamental geometric parameter values of the model.

Parameter	Value	Parameter	Value
Inner-tube diameter d/mm	22	Outer-tube diameter D/mm	50
Inner-tube wall thickness δ_{tube}/mm	1	Fin thickness δ/mm	1
Helix angle α/(°)	55	Helix pitch S/mm	100
Low-fin height h/mm	7	High-fin height H/mm	14

3. Mathematical model and boundary conditions

The numerical model is established based on the following assumptions. The working fluid is air and is treated as incompressible with constant thermophysical properties. A no-slip boundary condition is applied on all solid walls, and heat loss to the ambient is neglected. Turbulence is modeled using the renormalization-group (RNG) k-ε model [49], which improves upon the standard k–ε formulation by modifying the turbulent viscosity and providing an analytical expression for the turbulent Prandtl number. Owing to its reported robustness for flows with strong swirl and streamline curvature, the RNG k–ε model is adopted for the present finned DTHE simulations. Because the temperature range is moderate and the flow velocities are relatively low, thermal radiation and viscous dissipation are neglected. The governing equations,

with thermal radiation, viscous dissipation, and gravitational body forces neglected, are expressed as follows:

Continuity equation:

$$\frac{\partial(\rho v_i)}{\partial x_i} = 0 \tag{2}$$

Momentum equation for turbulent flow:

$$\frac{\partial}{\partial t}(\rho v_i) + \frac{\partial}{x_j}(\rho v_i v_j) = -\frac{\partial p}{\partial x_i} + \frac{\partial \tau_{ij}}{\partial x_j} \tag{3}$$

Energy equation for turbulent flow:

$$\frac{\partial(\rho T)}{\partial t} + div(\rho v T) = div\left(\frac{k}{c_p} grad T\right) \tag{4}$$

k and ε:

$$\frac{\partial}{\partial x_i}(\rho k u_i) = \frac{\partial}{\partial x_i}\left((\mu + \mu_i)\frac{\partial k}{\partial x_i}\right) + G_K - \rho\varepsilon \tag{5}$$

$$\frac{\partial}{\partial_i}(\rho \varepsilon u_i) = \frac{\partial}{\partial x_i}\left((\mu + \mu_i)\frac{\partial \varepsilon}{\partial x_i}\right) + C_{1\varepsilon}\frac{\varepsilon}{k}G_k - C_{2\varepsilon}\rho\frac{\varepsilon^2}{k} \tag{6}$$

$$\mu_t = \rho C_\mu \frac{k^2}{\varepsilon} \tag{7}$$

The model constants $C_{1\varepsilon}$, $C_{2\varepsilon}$, and C_μ are assigned values of 1.42, 1.68, and 0.0845, respectively.

The boundary conditions are summarized in tab. 2.

Tab. 2. Boundary conditions used in the numerical simulations.

Item	Boundary type	Value
Inlet (shell side)	Velocity inlet	T_{in} = 298 K, Re = 4,000–16,000
Outlet (shell side)	Pressure outlet	P_{out} = 0 Pa
Heated wall (inner tube)	Constant temperature wall	T_{wall} = 373 K
Outer wall (outer tube)	Adiabatic wall	0

Considering heat conduction in the helical fins, the fin surfaces are modeled as no-slip walls with thermal coupling. The annular passage formed by the inner tube, outer tube, and helical fins has a cross-section that can be approximated as rectangular along the helical direction. For complex non-circular passages, the hydraulic diameter is commonly used as the characteristic length for defining the Reynolds number and other dimensionless parameters [50]. In the high–low double-helical fin configuration, the contribution of the low-height fins must be explicitly included in the equivalent hydraulic diameter. Accordingly, the hydraulic diameter (D_e) is defined as follows:

$$D_e = \frac{4A}{L_p} \tag{8}$$

Reynolds number:

$$Re = \frac{\rho u_m D_e}{\mu} \tag{9}$$

The fanning friction factor is:

$$f = -\frac{D_e \left(\Delta P / \Delta l\right)}{2\rho u_m^2} \tag{10}$$

Heat transfer coefficient:

$$h_a = \frac{Q_{shell}}{A_0 \bullet \Delta T_{shell,m}} \tag{11}$$

$$Q_{shell} = M_{shell} C_{P,shell} \left(T_{shell,out} - T_{shell,in}\right) \tag{12}$$

Nusselt number:

$$Nu = \frac{h_a D_e}{\lambda} \tag{13}$$

The Performance Evaluation Criterion (*PEC*) provides a standardized approach for assessing the overall performance of a heat exchanger by balancing the enhancement in heat transfer against the associated changes in flow resistance. A *PEC* value greater than 1 indicates that, under comparable flow conditions, the improvement in heat transfer is more favorable relative to the incurred pressure drop, rather than implying an absolute simultaneous improvement in both heat transfer and flow resistance. The *PEC* is defined as follows [51]:

$$PEC = \frac{Nu / Nu_0}{(f / f_0)^{1/3}} \tag{14}$$

Where Nu_0 and f_0 refer to the average Nusselt number and friction factor of the conventional single helical fin DTHE, respectively.

4. Numerical methods and validation

The governing equations are discretized using the finite volume method, and pressure–velocity coupling is handled using the SIMPLE algorithm. The momentum and energy equations are solved with a second order upwind scheme, whereas the transport equations for turbulent kinetic energy k and dissipation rate ε are solved using a first order upwind scheme. To ensure numerical reliability while controlling computational cost, a mesh independence study is performed. Fig. 3 shows the variations of *Nu* and *f* for the discontinuous high–low fin model as a function of the total number of grid cells.

As shown in fig. 3, increasing the grid count from 221,596 to 2,331,823 cells leads to a noticeable increase in *Nu* and a corresponding decrease in *f*, indicating that meshes in this range

are not sufficiently refined to yield grid independent predictions. When the mesh is further refined from 2,331,823 to 3,917,653 cells, the changes in *Nu* and *f* become negligible. A quantitative comparison shows that the solution obtained with 2,331,823 cells differs from the 3,917,653-cell reference solution by approximately 0.7% in *Nu* and 0.3% in *f*. Considering both accuracy and computational cost, the mesh with 2,331,823 cells is selected for subsequent simulations (see fig. 4). Near wall turbulence is treated using the standard wall function approach, and the mean wall y^+ is 40.34, which is consistent with the adopted near wall treatment.

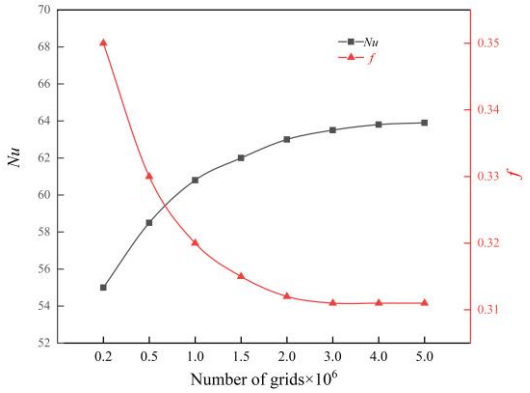

Fig. 3. Mesh independence verification

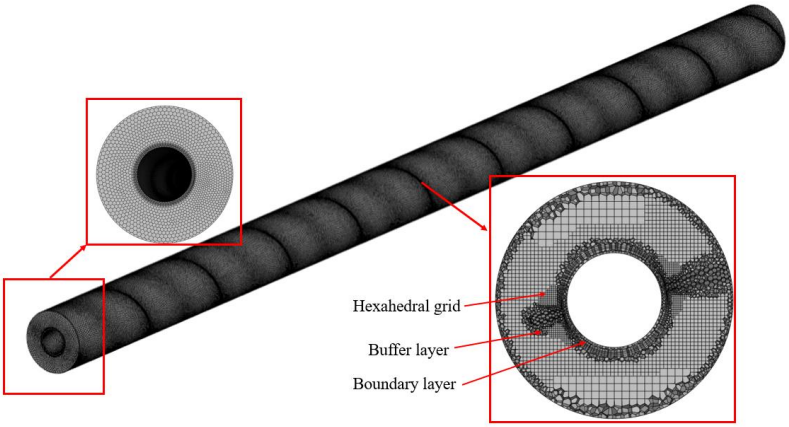

Fig. 4. Mesh generation of the computational domain

Model validation was conducted using established empirical correlations. Because no experimental data or dedicated correlations are available for the proposed discontinuous high–low double-helical fin configuration, the numerical approach was first applied to a conventional helical finned DTHE to reproduce annulus-side flow and heat transfer characteristics. The predicted *Nu* and *f* were compared with the experimental correlations reported by Zhang [52] (eqs. (15) and (16)). As shown in fig. 5, over the investigated *Re* range, the maximum deviation is below 12% for *Nu* and below 15% for *f*, indicating that the simulations capture the experimental trends with acceptable accuracy. The larger deviation in *f* may be attributed to modeling simplifications, such as neglecting the influence of fin surface roughness, as well as the greater difficulty of predicting pressure drop in helical annular flows. Moreover, the empirical correlations are fitted under specific experimental conditions, which may introduce additional uncertainty in the comparison.

To further assess the suitability of the turbulence model, additional simulations were conducted using several turbulence closures, including the Standard k–ε, Realizable k–ε, RNG k–ε, and SST k–ω models. The predicted Nu and f were compared with the experimental data, as shown in fig. 6.

As shown in fig. 6(a), the RNG k–ε model exhibits the closest agreement with the experimental Nu over the investigated Re range. The Standard and Realizable k–ε models show larger deviations at higher Re, whereas the SST k–ω model consistently underpredicts heat transfer. Similar trends are observed for the f in fig. 6(b). Overall, the RNG k–ε model provides the most balanced accuracy for both heat transfer and flow resistance and is therefore adopted for the subsequent parametric and optimization analyses.

$$Nu = 0.1414 Re^{0.6188} Pr^{0.4} \tag{15}$$

$$f = 1.0159 Re^{-0.3477} \tag{16}$$

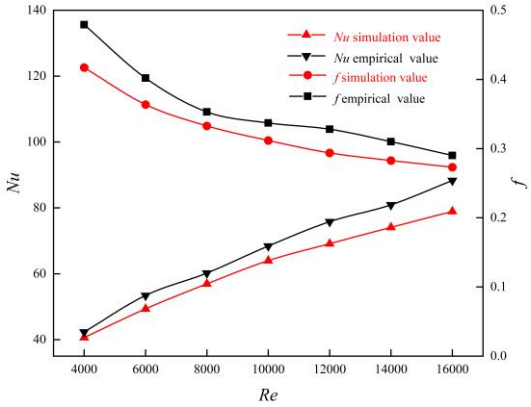

Fig. 5. Model validation

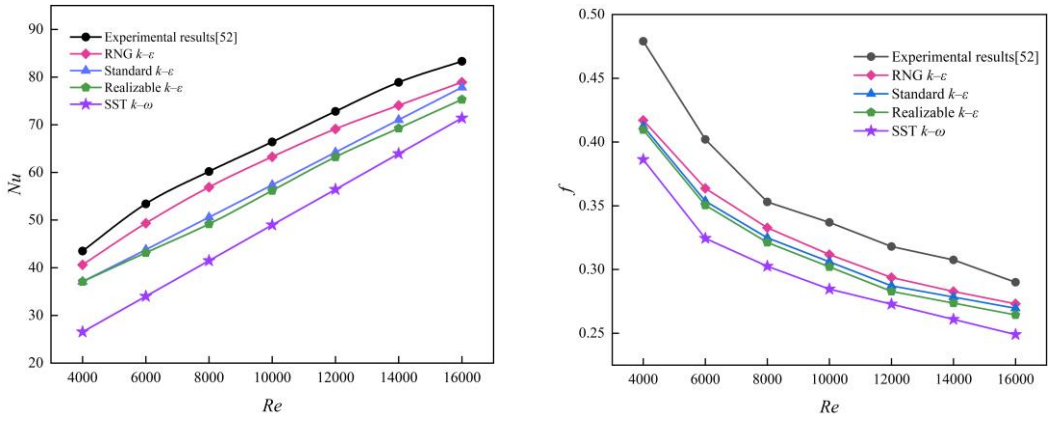

(a) *Nu* as a function of *Re* **(b) *f* as a function of *Re***

Fig. 6. Experimental vs numerical results for different turbulence models

5. Analysis of the effects of structure on flow and heat transfer characteristics

5.1 Analysis of shell-side flow and heat transfer characteristics

Fig. 7 presents the velocity contours on the Y-plane for the two fin configurations. The sectional mean velocity is 7.7 m/s for the conventional single helical fin configuration (fig. 7(a)) and 7.5 m/s for the discontinuous high–low double-helical fin configuration (fig. 7(b)). For the conventional configuration, the velocity field is markedly non-uniform. A substantial portion of the cross-section is occupied by low-velocity regions (approximately 2–5 m/s), mainly located near the central part of the annulus, whereas higher velocities are concentrated in the vicinity of the fin surfaces. This pattern is attributable to the continuous helical passage, which sustains centrifugal effects and promotes velocity stratification.

By contrast, the discontinuous high–low double-helical fin configuration exhibits a more compact velocity distribution, with most of the flow remaining within a moderate range of approximately 5–8 m/s. The reduction in low-velocity regions indicates that dead-flow zones are effectively suppressed. Although the sectional mean velocity is slightly lower, the overall field becomes more uniform due to enhanced momentum redistribution induced by axial interruptions and fin-height variation.

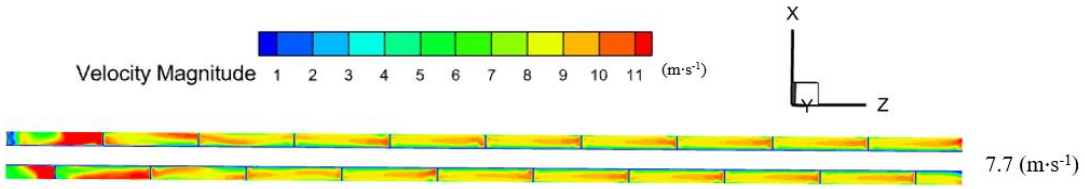

(a) Conventional single helical fins

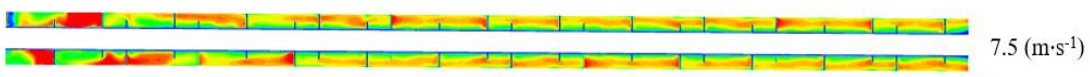

(b) Discontinuous high-low double-helical fins

Fig. 7. Velocity distribution on the Y-plane for the two configurations

Fig. 8 presents the temperature contours on the Y-plane for the two fin configurations. The sectional mean temperature is 326 K for the conventional single helical fin configuration (fig. 8(a)) and increases to 332 K for the discontinuous high–low double-helical fin configuration (fig. 8(b)). In the conventional configuration, the temperature field remains relatively low and exhibits noticeable non-uniformity, especially in regions away from the inner tube where extensive low-temperature zones persist. By contrast, the discontinuous high–low double-helical fin configuration produces a higher and more uniformly distributed temperature field across the annulus.

The contours indicate that the medium-to-high temperature range (approximately 330–350 K) occupies about two-thirds of the cross-sectional area for the discontinuous high–low double-helical fin configuration, whereas it accounts for only about one-third in the conventional configuration. This suggests that the discontinuous high–low design substantially enlarges the effective heat transfer region and improves thermal uniformity within the annulus.

These improvements are attributed to the combined effects of increased effective fin surface area and a periodically interrupted, height-varying helical flow path, which promotes flow redistribution and disrupts the thermal boundary layer. Consequently, heat transfer is enhanced

throughout the annular region, leading to improved temperature uniformity and overall thermal performance.

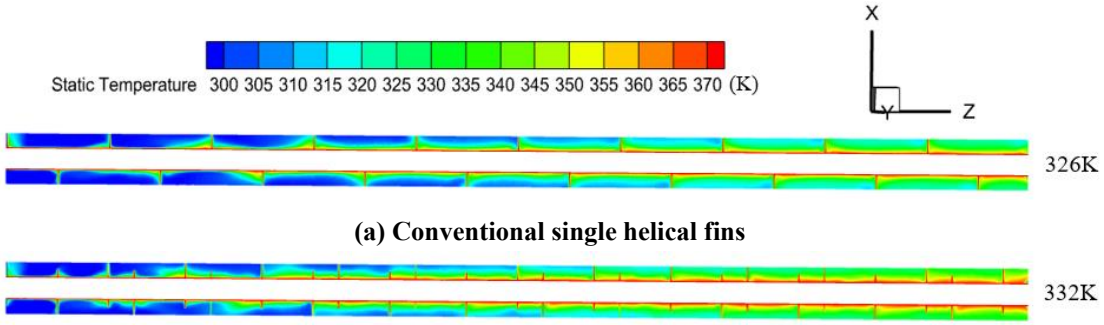

(a) Conventional single helical fins

(b) Discontinuous high-low double-helical fins

Fig. 8. Temperature distribution on the Y-plane for the two configurations

5.2 Response trends of average Nusselt number and friction factor

Fig. 9(a) compares *Nu* for the conventional single helical fin configuration and the discontinuous high–low double-helical fin configuration over the investigated *Re* range. For both configurations, *Nu* increases with *Re*. The difference between the two cases widens with *Re*, increasing from approximately 2.03 at *Re* = 4,000 to approximately 15.25 at *Re* = 16,000. Across the studied range, the discontinuous high–low configuration yields *Nu* values that are about 5%–19% higher than those of the conventional configuration, with the largest relative improvements at higher *Re*. This indicates that the interrupted high–low geometry is particularly effective under stronger flows, owing to enhanced turbulence generation and intensified near-wall mixing.

Fig. 9(b) compares the friction factor *f* for the two configurations. For both designs, *f* decreases with increasing *Re*. Over the examined range, *f* for the discontinuous high–low configuration remains higher than that for the conventional configuration, decreasing from about 0.47 at *Re* = 4,000 to about 0.30 at *Re* = 16,000, compared with a decrease from about 0.41 to about 0.27 for the conventional configuration. The corresponding difference narrows from approximately 0.058 at *Re* = 4,000 to approximately 0.029 at *Re* = 16,000, as viscous effects become less dominant at higher *Re*.

To provide quantitative support for the turbulence-based interpretation, fig. 10 presents the volume-averaged turbulent kinetic energy k as a function of Re for both configurations. As Re increases, k increases monotonically in both cases, and the discontinuous high–low double-helical fin configuration consistently exhibits higher k values than the conventional single helical fin configuration. This indicates a higher turbulence level and stronger mixing induced by the proposed geometry, which benefits heat transfer but also increases momentum dissipation, contributing to the higher friction factor observed in fig. 9(b).

The higher *f* of the discontinuous high–low configuration can be attributed to the increased flow path complexity and elevated turbulence intensity, together with more frequent local accelerations and decelerations. These features may promote separation and vortex formation at fin discontinuities and, combined with the larger wetted surface area, lead to increased pressure losses. Overall, the proposed design enhances *Nu* but also increases *f*, highlighting the interplay between heat transfer augmentation and flow resistance.

The observed performance trends of the discontinuous high–low double-helical fin configuration can be attributed to the combined effects of fin discontinuity, alternating fin height, and helix angle. Axial fin discontinuity introduces periodic disturbances that promote repeated redevelopment of the velocity and thermal boundary layers and mitigate the velocity stratification typical of continuous helical passages. Alternating high and low fin heights enhance local shear and momentum redistribution, thereby improving mixing and heat transfer uniformity while avoiding excessive flow blockage. Meanwhile, the helix angle regulates the strength of secondary swirling flow and thus governs the interplay between heat transfer enhancement and pressure loss. Together, these mechanisms provide a consistent physical explanation for the variations in *Nu* and *f* observed in this section and support the interpretation of the *PEC* discussed in the subsequent optimization analysis.

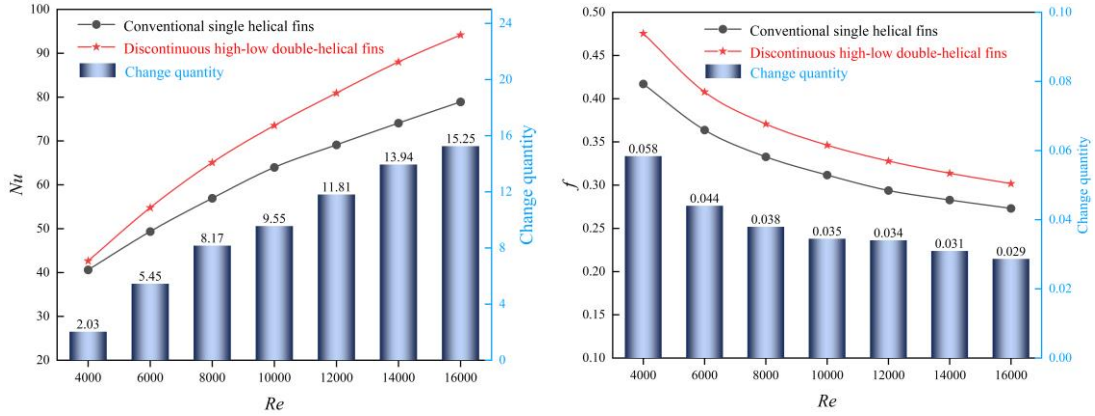

(a) Comparison of *Nu* for the two fin configurations **(b) Comparison of *f* for the two fin configurations**

Fig. 9. Variations of *Nu* and *f* with *Re* for the conventional single helical fin and discontinuous high–low double-helical fin configurations.

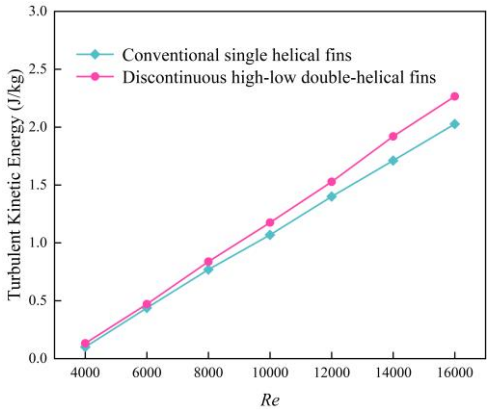

Fig. 10. Variation of annulus volume-averaged turbulent kinetic energy with *Re* for the two configurations.

5.3 Field synergy analysis

Based on the field synergy theory proposed by Academician Guo Zengyuan [53], convective heat transfer depends not only on fluid velocity, thermophysical properties, and the temperature difference at the solid-fluid interface, but also on the degree of alignment between the velocity vector field and the temperature-gradient vector field [54]. A larger cosine of the

angle between the velocity vector and the temperature gradient, that is, a smaller synergy angle β ($\beta < 90°$), corresponds to closer alignment of the two fields. Enhanced field synergy is associated with improved convective heat transfer performance. The synergy angle (β) is defined as [55]:

$$\beta = \arccos \frac{U \cdot \nabla T}{|U||\nabla T|} \tag{17}$$

In the present study, the reported synergy angle is obtained by volume-averaging the local values over the effective heat transfer region. The local synergy angle in each computational cell is calculated by extracting the cell-wise velocity vector and temperature gradient using User Defined Functions (UDF).

At *Re* = 10,000, the distribution of the field synergy angle on the XY plane at Z = 500 mm is shown in fig. 11. In fig. 11(a), the contour field is relatively uniform, with a large area occupied by high-angle regions, whereas fig. 11(b) exhibits a more heterogeneous pattern with a greater proportion of low-angle regions. This indicates that the discontinuous high–low double-helical fins, owing to their staggered and periodically interrupted geometry, enhance turbulence and mixing, thereby improving the alignment between the velocity field and the temperature-gradient field and yielding smaller synergy angles. According to field synergy theory, smaller synergy angles correspond to stronger field alignment and improved convective heat transfer, which helps explain the enhanced heat transfer performance of the discontinuous high–low configuration relative to the conventional single helical fin configuration.

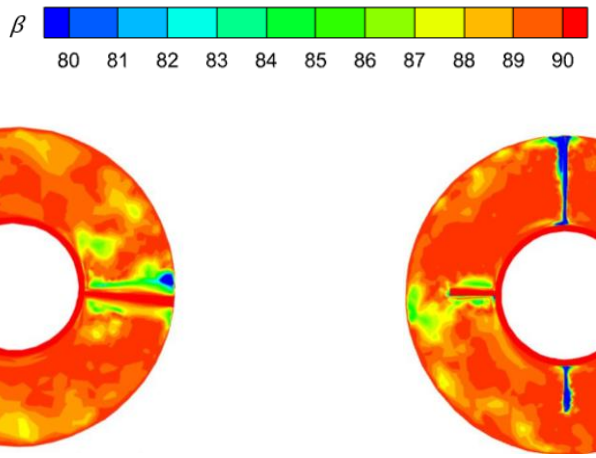

(a) Conventional single helical fins **(b) Discontinuous high-low double-helical fins**

Fig. 11. Local distribution of the synergy angle on the XY plane at Z = 500 mm (*Re* = 10,000)

6. Response Surface Methodology optimization study

RSM is a statistical optimization technique that constructs a surrogate model from a limited number of experiments or simulations to establish relationships between design variables and performance indicators for prediction and optimization. In heat transfer research, RSM has also been integrated with data-driven surrogate modeling to improve response prediction and enable efficient optimization [56, 57].

6.1 Influence of single-factor variations on heat transfer performance

Single-factor experiments represent the initial stage of RSM and are used to evaluate the effect of an individual input variable on the response while keeping the other variables constant [58]. In each test, the selected variable is varied systematically and the corresponding response in *Nu* is recorded, which provides a preliminary indication of parameter importance and helps determine suitable ranges for subsequent optimization. In the present study, the investigated factors are the fin discontinuity distance (S), low-fin height (h), and helix angle (α). The parameter ranges used in the single-factor analysis are chosen based on physical feasibility, geometric constraints, and practical manufacturability, and are intended to define a reasonable design space for the subsequent RSM optimization. Figs. 12–14 show the effects of these factors on *Nu* for the discontinuous high–low double-helical fin DTHE at Re = 10,000.

Fig. 12 shows that *Nu* first increases and then decreases as S increases. When S increases from 0 to 100 mm, *Nu* rises gradually and reaches a maximum at S = 100 mm. With a further increase in S from 100 to 500 mm, *Nu* decreases monotonically. Accordingly, a design range of S = 0–200 mm is recommended to obtain favorable heat transfer performance.

Fig. 13 shows a non-monotonic influence of h on *Nu*. The variation in *Nu* is small for h = 1–4 mm, increases to a peak value of 80.46 at h = 12 mm, and then decreases to 77.72 at h = 14 mm, which is likely associated with reduced turbulence intensity and weakened mixing at larger h. Therefore, h = 10–14 mm is suggested.

A similar trend is observed in fig. 14: *Nu* increases as α increases from 45° to 55°, reaches a maximum at α = 55°, and then decreases as α increases further to 65°. Consequently, α = 50°–60° is recommended.

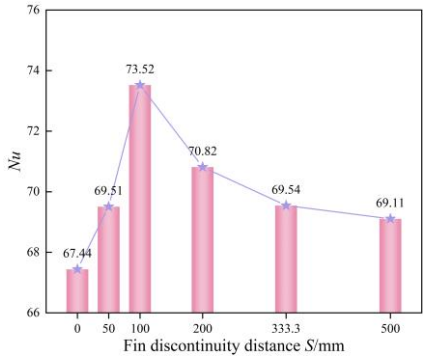

Fig. 12. Effect of *S* on *Nu*

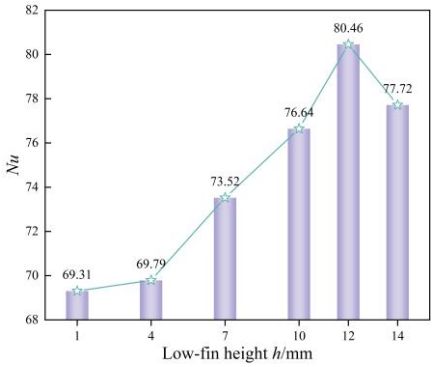

Fig. 13. Effect of *h* on *Nu*

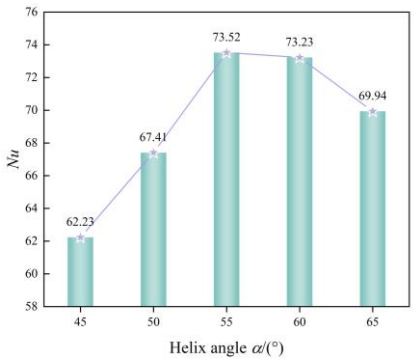

Fig. 14. Effect of *α* on *Nu*

6.2 Model construction and variance significance analysis

Based on the single-factor experiments, the design variables and their levels are listed in tab. 3. A Box–Behnken design with three factors at three levels was adopted, yielding 17 runs. The simulation results were then substituted into eqs. (8)–(14) to calculate *Nu*, and the outcomes are summarized in tab. 4. Repeated center-point runs were included to estimate numerical error and to assess the reproducibility and adequacy of the response surface model.

Tab. 3. Factors and levels for Box Behnken design

Level	A	B	C
	Fin discontinuity distance *S*/mm	Low-fin height *h*/mm	Helical angle α/(°)
-1	0	10	50
0	100	12	55
1	200	14	60

Tab. 4. Box Behnken design and results

Run number	A	B	C	*Nu*
1	200	12	50	71.33
2	0	12	50	70.91
3	0	10	55	72.17
4	100	12	55	80.46
5	100	10	50	72.89
6	200	14	55	77.17
7	200	12	60	80.64
8	100	12	55	80.46
9	200	10	55	77.11
10	100	10	60	78.47
11	100	14	50	71.85
12	100	12	55	80.46
13	0	14	55	73.28
14	100	14	60	80.29
15	0	12	60	75.60
16	100	12	55	80.46
17	100	12	55	80.45

For the discontinuous high–low double-helical finned DTHE, an analysis of variance (ANOVA) was performed using Design-Expert 13, and a quadratic polynomial regression model was fitted to describe the relationship between the response indicators and the structural parameters. This correlation is valid only within the parameter ranges and operating conditions investigated in this study. The resulting regression equation is given as follows:

$$\begin{aligned} Nu = &-297.32583 - 0.02541A + 9.12472B + 10.37903C \\ &-0.001315AB + 0.002306AC + 0.071655BC \\ &-0.00339A^2 - 0.533862B^2 - 0.097901C^2 \end{aligned} \tag{18}$$

A comparison between *Nu* values predicted by the response surface model and those

obtained from simulations is presented in fig. 15. The solid line denotes the model prediction, and the symbols represent the simulation data. The deviation remains within 5%, indicating good agreement between the RSM predictions and the CFD results.

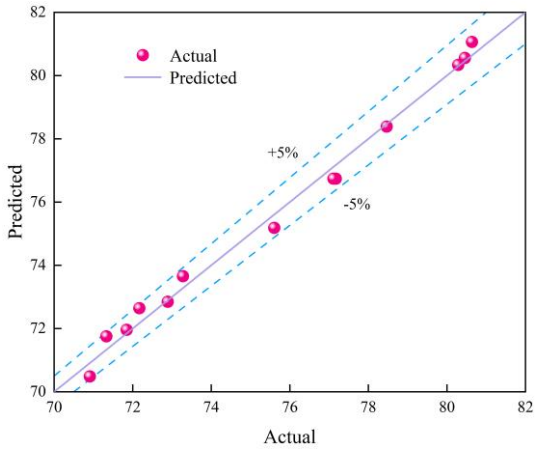

Fig. 15. Comparison of predicted and actual values (RSM)

Tab. 5. ANOVA results for the regression model

Source	Sum of squares	Degrees of freedom	Mean square	F value	P value
Model	234.8	9	26.09	126.46	<0.0001
A	25.51	1	25.51	123.64	<0.0001
B	0.4731	1	0.4731	2.29	0.1737
C	98.09	1	98.09	475.5	<0.0001
AB	0.2766	1	0.2766	1.34	0.2849
AC	5.32	1	5.32	25.77	0.0014
BC	2.05	1	2.05	9.96	0.016
A^2	48.34	1	48.34	234.33	<0.0001
B^2	19.2	1	19.2	93.07	<0.0001
C^2	25.22	1	25.22	122.26	<0.0001
Residual	1.44	7	0.2063		
Lack of Fit	1.44	3	0.4814		
Cor total	236.24	16			
R^2 =	Adjusted R^2 =	Predicted R^2 =	Std. Dev. =	C. V. =	Adeq Precision =
0.9939	0.986	0.9022	0.4542	0.5921%	30.3555

The model coefficients were estimated using the least-squares method in Design-Expert 13, and the corresponding ANOVA results are summarized in tab. 5. The statistical metrics indicate an excellent fit of the quadratic model (R^2 = 0.9939, adjusted R^2 = 0.9860) and good predictive capability (predicted R^2 = 0.9022). In addition, the residual standard deviation is 0.4542, the coefficient of variation is 0.5921%, and Adeq Precision is 30.3555, indicating adequate model accuracy and a strong signal-to-noise ratio within the investigated ranges.

As shown in tab. 5, the overall model is highly significant ($F = 126.46$, $P < 0.0001$). Here,

A, B, and C denote the fin discontinuity distance, low-fin height, and helix angle, respectively; AB, AC, and BC are interaction terms, and A^2, B^2, and C^2 are quadratic terms. Factors A and C are significant ($P < 0.0001$), whereas B is not significant as a main effect ($P = 0.1737$). The interaction terms AC and BC are significant ($P < 0.05$), while AB is not ($P = 0.2849$). All quadratic terms are significant ($P < 0.05$), confirming pronounced nonlinear effects.

Based on the F values, C (helix angle) has the strongest influence ($F = 475.50$), followed by A^2 ($F = 234.33$), A ($F = 123.64$), C^2 ($F = 122.26$), and B^2 ($F = 93.07$). The interaction terms AC ($F = 25.77$) and BC ($F = 9.96$) are smaller but still influential, whereas B ($F = 2.29$) and AB ($F = 1.34$) are not significant. Overall, the factor importance for *Nu* ranks as C > A > B (helix angle > fin discontinuity distance > low-fin height).

In the discontinuous high–low double-helical finned DTHE, the helix angle (C) is the most influential factor affecting *Nu*, and both its linear and quadratic terms are statistically significant. The fin discontinuity distance (A) also exhibits significant linear and nonlinear effects, indicating that A should be optimized to balance hydraulic losses and heat transfer enhancement. The low-fin height (B) has a relatively small main effect on *Nu* within the investigated range; however, its interaction with C is significant, suggesting that the influence of B is primarily expressed through interaction effects rather than as an independent dominant factor. Therefore, the optimization should prioritize the helix angle, subsequently adjust the fin discontinuity distance to achieve a suitable balance between pressure drop and heat transfer, and finally consider the interactions among A, B, and C to obtain the best overall thermal performance.

In summary, the fitted quadratic model captures the primary trends in the simulation results and is suitable for predicting heat transfer performance within the investigated parameter space. It therefore provides a reliable basis for response-surface optimization and subsequent design refinement.

Fig. 16(a) presents the response surface and contour plot of A versus B for *Nu*. *Nu* increases with B to a maximum and then decreases, indicating a pronounced nonlinear effect and an optimal B. The variation along the A direction is milder, and the nearly elliptical, relatively flat contours suggest a weak AB interaction, with B exerting the dominant influence.

Fig. 16(b) shows the response surface and contour plot for A versus C. *Nu* increases markedly with C, and the surface exhibits strong curvature along the C direction, indicating the presence of an optimal helix angle. The contour lines become denser at higher C and show a clear AC interaction, whereas the wider spacing along the A axis reflects the weaker main effect of A. A closed contour region identifies an extremum at high C combined with a moderate A.

Fig. 16(c) presents the response surface and contour plot for B versus C. The surface further confirms that C has the strongest positive effect on *Nu*. The contours are generally elliptical, and their relative flattening (fig. 16(a) < fig. 16(c) < fig. 16(b)) indicates the interaction-strength ordering AC > BC > AB, consistent with tab. 5.

The optimized structural parameters for the discontinuous high–low double-helical fin DTHE are: $S = 142.5$ mm, $h = 12.1$ mm, and $\alpha = 59.3°$. Under the specified conditions, the response surface model predicts $Nu = 82.24$.

To verify the feasibility of the predicted optimal parameters, a CFD model of the discon-

tinuous high–low double-helical fin DTHE was constructed using the optimal parameter combination obtained from the RSM optimization. The geometric configuration, meshing strategy, and boundary conditions were kept identical to those of the unoptimized model to ensure a fair comparison. The *Nu* for the optimized configuration was obtained from CFD and compared with both the unoptimized model and the RSM prediction; the results are summarized in tab. 6.

As shown in tab. 6, the relative deviation between the CFD result for the optimized configuration and the RSM-predicted value is only 0.5%, indicating high predictive accuracy. Moreover, relative to the unoptimized model, the optimized discontinuous high–low double-helical fin DTHE achieves an 11.3% increase in *Nu*. These results confirm the reliability of the regression model linking the structural parameters to *Nu* and demonstrate the effectiveness of RSM for structural parameter optimization of this type of heat exchanger.

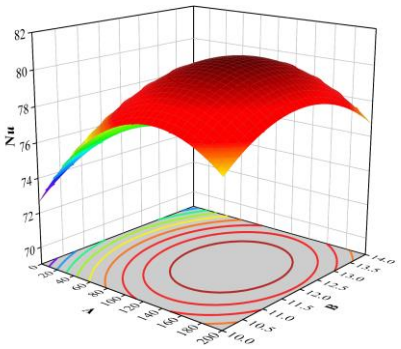

(a) Influence of factors A and B on *Nu*

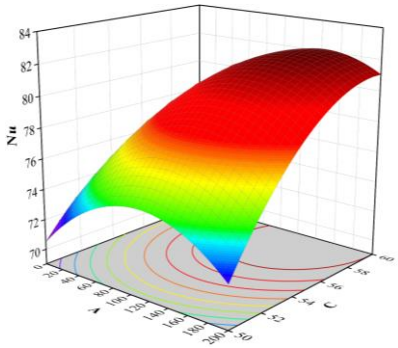

(b) Influence of factors A and C on *Nu*

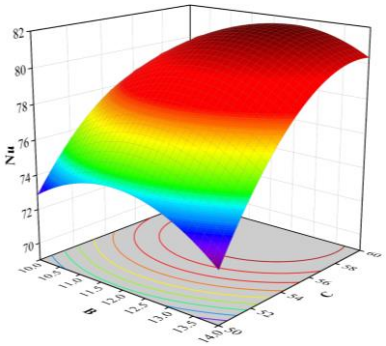

(c) Influence of factors B and C on *Nu*

Fig. 16. Response surface and contour plots

Tab. 6. Structural parameters and *Nu* values before and after optimization

	S/mm	*h*/mm	*α*/°	*Nu*
Before optimization	100	7	55	73.52
Optimized (Predicted value)	142.5	12.1	59.3	82.24
Optimized (CFD-calculated value)	142.5	12.1	59.3	81.81

6.3 PEC improvement assessment

For comparison, the proposed configuration and the conventional single helical fin heat exchanger use identical geometric dimensions, material properties, and operating conditions.

Fig. 17 shows *PEC* as a function of *Re* for the conventional single helical fin case, the unoptimized model, and the optimized discontinuous high–low double-helical fin DTHE. Across the investigated *Re* range, the optimized configuration consistently yields the highest *PEC*, and its advantage increases with *Re*. Compared with the conventional single helical fin configuration, the optimized design increases *Nu* by 28.25% and reduces *f* by 9.68%, resulting in a *PEC* of approximately 1.38. Relative to the unoptimized model, it increases *Nu* by 11.3%, reduces *f* by 20%, and improves *PEC* by 19.8%.

To place the present results in the context of existing research, a benchmark comparison was conducted against the helical finned DTHE reported by El Maakoul et al. [59]. The comparison was performed in terms of *PEC* using a consistent definition and matched operating and boundary conditions within the same numerical framework. As shown in fig. 18, the proposed discontinuous high–low double-helical fin configuration yields consistently higher *PEC* values across the investigated *Re* range.

After structural optimization, the discontinuous high–low double-helical fin design enhances heat transfer while reducing flow resistance, leading to a substantial increase in *PEC*. Increasing the low-fin height enlarges the effective heat transfer area and improves heat transfer capability. A larger helix angle strengthens circumferential guidance and induces more intense secondary disturbances, thereby promoting heat transport between the core flow and the near-wall region. In addition, increasing the fin pitch reduces fin density per unit length, alleviates flow blockage, and lowers pressure losses. As a result, heat transfer performance is improved without a proportional increase in pressure drop.

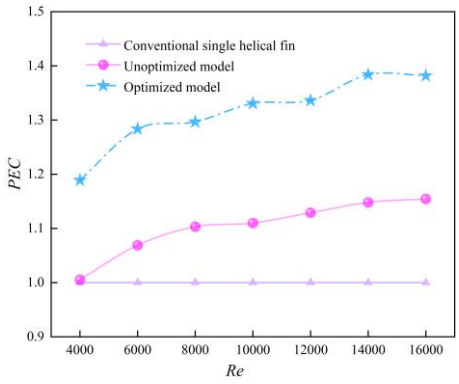

Fig. 17. *PEC* vs. *Re* for three helical fin configurations

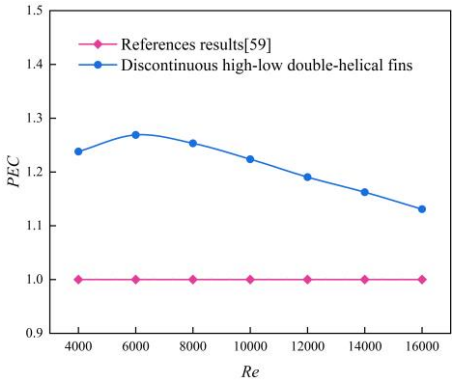

Fig. 18. *PEC* comparison with El Maakoul et al. [59]

7. Conclusion

This study proposes a discontinuous high–low double-helical fin configuration in a DTHE to enhance heat transfer while limiting the pressure-drop penalty. Numerical simulations were conducted to evaluate shell-side flow and heat transfer characteristics. RSM was then employed to optimize the helical angle α, low-fin height h, and fin-discontinuity distance S, yielding an optimal parameter combination. The principal conclusions are as follows:

(1) The proposed discontinuous high–low double-helical fins introduce periodic disturbances and alternating fin heights, which intensify mixing and improve flow redistribution in the

annulus. Consequently, low-velocity regions and dead-flow zones are reduced, and the shell-side velocity field becomes more uniform.

(2) Over Re = 4,000–16,000, the proposed configuration provides a net performance benefit. Compared with the conventional single helical fin configuration, Nu increases by 5.0%–19.3%, accompanied by a moderate increase in f of 10.4%–14.0%. The reduced volume-averaged synergy angle β supports the interpretation that improved alignment between the velocity and temperature-gradient fields contributes to enhanced convection.

(3) The geometric effects are nonlinear and coupled. The helical angle α plays the dominant role in balancing heat transfer and pressure loss, whereas h and S primarily regulate disturbance intensity and local loss generation. In practice, performance tuning should prioritize α, followed by coordinated adjustment of h and S to avoid excessive blockage while maintaining effective periodic disturbance.

(4) According to the response surface analysis, the model demonstrates strong statistical significance. The optimal parameter combination is S = 142.5 mm, h = 12.1 mm, and α = 59.3° at Re = 10,000. Under these optimal conditions, the optimized discontinuous high-low double-helical fin configuration yields an 11.3% increase in Nu, a 20% reduction in f, and a 19.8% improvement in PEC compared with the unoptimized design.

Future work will extend the present numerical analysis to additional working fluids to further assess the influence of fluid properties on the performance of the proposed configuration. Practical deployment will also require consideration of operating constraints and maintainability in waste-heat recovery environments.

Acknowledgment: This research was supported by the 2022 China National Textile and Apparel Council Science and Technology Guidance Plan Project (2022062).

Data Availability Statement: The raw data supporting the conclusions of this article will be made available by the authors on request.

Nomenclature

A	Total heat transfer area (mm^2)	u_m	Shell-side average flow velocity (m/s)
C_p	Specific heat capacity (kJ/(kg·K))	W	Flow channel height (mm)
DTHE	Double-tube heat exchanger	u, v, w	Components of velocity vector (m/s)
d	Inner tube diameter (mm)	x, y, z	Coordinates
D	Outer tube diameter (mm)	*Geek symbols*	
D_e	Hydraulic diameter (mm)	k	Turbulence kinetic energy (m^2/s^2)
f	Friction factor	ε	Turbulent dissipation rate
G_k	Turbulence production term	λ	Thermal conductivity (W/(m·K))
h	Height of low fins (mm)	ρ	Density (kg/m^3)
H	Height of high fins (mm)	δ	Thickness of fins (mm)
Hs	Pitch of helical fins (mm)	μ	Dynamic viscosity (kg/(m·s))
h_a	Heat transfer coefficient (W/(m^2·K))	α	Helical angle (°)
L	Effective length of heat exchanger	β	Synergy angle (°)

	(mm)		
ΔL	Length of the helical channel (mm)		
m	Mass flow rate (kg/s)	*Subscripts*	
Nu	Nusselt number	in	Inlet
P	Pressure (Pa)	*i, j, k*	Directions of the coordinate system
ΔP	Pressure drop (Pa)	fins	Helical fin surface
PEC	Performance evaluation criteria	out	Outlet
Q	Heat transfer rate (W)	outer	Outer tube wall
Re	Reynolds number	shell	Shell-side
S	Fin gap distance (mm)	0	Value of double tube with single helical fin
T	Temperature (K)		

References

[1] Hasgul, C., Cakmak, G., Heat Transfer Analysis of Double Tube Heat Exchanger with Wavy Inner Tube, *Thermal Science*, *26* (2022), 4B, pp. 3455-3462, DOI: 10.2298/TSCI210628266H

[2] Soundararajan, S., Selvaraj, M., Investigations of Protracted Finned Double Pipe Heat Exchanger System for Waste Heat Recovery from Diesel Engine Exhaust, *Thermal Science*, *27* (2023), 5, Part A, pp. 3783-3793, DOI: 10.2298/TSCI230212143S

[3] Omidi, M., *et al.*, A Comprehensive Review on Double Pipe Heat Exchangers, *Applied Thermal Engineering*, *110* (2017), pp. 1075-1090, DOI: 10.1016/j.applthermaleng.2016.09.027

[4] He, L., Li, P., Numerical Investigation on Double Tube-Pass Shell-and-Tube Heat Exchangers with Different Baffle Configurations, *Applied Thermal Engineering*, *143* (2018), pp. 561-569, DOI: 10.1155/2011/839468

[5] Ajarostaghi, S. S. M., *et al.*, Numerical Evaluation of the Impact of Using Spiral Innovative Turbulator on Improving the Thermal Performance of a Helical Double-Pipe Heat Exchanger, *International Journal of Thermofluids*, *24* (2024), pp. 100830, DOI: 10.1016/j.ijft.2024.100830

[6] Reheem, Z. A., *et al.*, Advances in Heat Pipe Technologies for Different Thermal Systems Applications: A Review, *Journal of Thermal Analysis and Calorimetry*, *147* (2022), 23, pp. 13011-13026, DOI: 10.1007/s10973-022-11660-6

[7] Mathry, A. H., *et al.*, Impact of Design and Operating Parameters on the Thermal Performance of Heat Pipes: A Review, *Journal of Engineering Research*, *13* (2025), 2, pp. 985-1000, DOI: 10.1016/j.jer.2024.02.004

[8] Sun, Y., *et al.*, Experimental Study on Serpentine-Looped Minichannel Pulsating Heat Pipe Heat Exchanger with Horizontal Installation for Full-Year Efficient Heat Recovery in Air Conditioning, *International Journal of Refrigeration*, (2025), DOI: 10.1016/j.ijrefrig.2025.06.019

[9] Amiri Delouei, A., *et al.*, Louvered Fin-and-Flat Tube Compact Heat Exchanger under Ultrasonic Excitation, *Fire*, *6* (2022), 1, pp. 13, DOI: 10.3390/fire6010013

[10] Delouei, A. A., *et al.*, The Thermal Effects of Multi-Walled Carbon Nanotube Concentration on an Ultrasonic Vibrating Finned Tube Heat Exchanger, *International Communications in Heat and Mass Transfer*, *135* (2022), pp. 106098, DOI: 10.1016/j.icheatmasstransfer.2022.106098

[11] Jalali, A., *et al.*, Experimental Investigation on Active Heat Transfer Improvement in Double-Pipe

Heat Exchangers, *Processes*, *12* (2024), 7, pp. 1333, DOI: 10.3390/pr12071333
[12] Kadhim, S. A., *et al.*, Increasing the Thermal Performance of Double-Pipe Heat Exchangers by Active Methods: A Comprehensive Review, *International Communications in Heat and Mass Transfer*, *169* (2025), pp. 109837, DOI: 10.1016/j.icheatmasstransfer.2025.109837
[13] Liu, S., *et al.*, Experimental Investigation on Shell-Side Performance of a Novel Shell and Tube Oil Cooler with Twisted Oval Tubes, *International Journal of Thermal Sciences*, *152* (2020), pp. 106290, DOI: 10.1016/j.ijthermalsci.2020.106290
[14] Barati, S., *et al.*, Heat Transfer and Fluid Flow Characteristics of a Dual-Tube Heat Exchanger with Alternating Flattened Tubes, *Journal of Thermal Analysis and Calorimetry*, *149* (2024), 23, pp. 13967-13980, DOI: 10.1007/s10973-024-13614-6
[15] Al-Obaidi, A. R., Alhamid, J., Investigation of Flow Pattern, Thermohydraulic Performance and Heat Transfer Improvement in 3D Corrugated Circular Pipe under Varying Structure Configuration Parameters with Development Different Correlations, *International Communications in Heat and Mass Transfer*, *126* (2021), pp. 105394, DOI: 10.1016/j.icheatmasstransfer.2021.105394
[16] Alhamid, J., Al-Obaidi, R. A., Flow Pattern Investigation and Thermohydraulic Performance Enhancement in Three-Dimensional Circular Pipe under Varying Corrugation Configurations, *Journal of Physics: Conference Series*, *1845* (2021), 1, pp. 012061, DOI: 10.1088/1742-6596/1845/1/012061
[17] Wu, J., *et al.*, Numerical Research of an Internal and External-Corrugated Tube-in-Tube Helical Coil Heat Exchanger, *Energy Sources, Part A: Recovery, Utilization, and Environmental Effects*, *46* (2024), 1, pp. 3581-3600, DOI: 10.1080/15567036.2024.2319724
[18] Abdelmagied, M., Determining of the Thermo-Hydraulic Characteristics and Exergy Analysis of a Triple Helical Tube with Inner Twisted Tube, *Chemical Engineering and Processing–Process Intensification*, *204* (2024), pp. 109922, DOI: 10.1016/j.cep.2024.109922
[19] Abdelmagied, M., Thermo-Fluid Characteristics and Exergy Analysis of a Twisted Tube Helical Coil, *Scientific Reports*, *14* (2024), 1, pp. 27873, DOI: 10.1038/s41598-024-78164-1
[20] Abdelmagied, M., Thermo-Hydraulic and Exergy Characteristics of a Triple Tube Helical Coil with Inner Triangular Twisted Tube, *International Journal of Air-Conditioning and Refrigeration*, *32* (2024), 1, pp. 21, DOI: 10.1007/s44189-024-00065-9
[21] Abdelmagied, M., Investigation of a Tube in Tube Conically Coil Heat Exchanger Thermal and Fluid Flow Performance Characteristics, *International Journal of Air-Conditioning and Refrigeration*, *33* (2025), 1, pp. 1-18, DOI: 10.1007/s44189-025-00071-5
[22] Abdelmagied, M., Fluid and Thermal Flow in Annular Side of the Double Twisted Helically Coiled Tubes Heat Exchangers under Various Configurations, *International Journal of Air-Conditioning and Refrigeration*, *33* (2025), 1, pp. 17, DOI: 10.1007/s44189-025-00084-0
[23] Abdelmagied, M., Investigation of Fluid Flow and Heat Transfer in Annulus Conical Tubes, *Discover Applied Sciences*, *8* (2025), pp. 128, DOI: 10.1007/s42452-025-07974-3
[24] Kadhim, S. A., *et al.*, Influence of the Typical Twisted Tape Inserts into the Inner Tube of Double-Pipe Heat Exchanger: A Limited Review, *Results in Engineering*, (2025), pp. 104386, DOI: 10.1016/j.rineng.2025.104386
[25] Kadhim, S. A., *et al.*, Enhancing the Thermal Performance of Double-Pipe Heat Exchangers Using Wire Coil Inserts: A Focused Review, *Scientific African*, (2025), pp. e2896, DOI: 10.1016/j.sciaf.2025.e02896
[26] Chaurasia, S. R., Sarviya, R. M., Thermal Performance Analysis of CuO/Water Nanofluid Flow in

a Pipe with Single and Double Strip Helical Screw Tape, *Applied Thermal Engineering*, *166* (2020), pp. 114631, DOI: 10.1016/j.applthermaleng.2019.114631

[27] Hussein, M. A., Hameed, V. M., Experimental Investigation on the Effect of Semi-Circular Perforated Baffles with Semi-Circular Fins on Air–Water Double Pipe Heat Exchanger, *Arabian Journal for Science and Engineering*, *47* (2022), 5, pp. 6115-6124, DOI: 10.1007/s13369-021-05869-0

[28] Barzegar, A., Jalali Vahid, D., Numerical Study on Heat Transfer Enhancement and Flow Characteristics of Double Pipe Heat Exchanger Fitted with Rectangular Cut Twisted Tape, *Heat and Mass Transfer*, *55* (2019), 12, pp. 3455-3472, DOI: 10.1007/s00231-019-02667-1

[29] Demir, H., *et al.*, Numerical Investigation on the Single Phase Forced Convection Heat Transfer Characteristics of TiO_2 Nanofluids in a Double-Tube Counter Flow Heat Exchanger, *International Communications in Heat and Mass Transfer*, *38* (2011), 2, pp. 218-228, DOI: 10.1016/j.icheatmasstransfer.2010.12.009

[30] Chandra Sekhara Reddy, M., Vasudeva Rao, V., Experimental Investigation of Heat Transfer Coefficient and Friction Factor of Ethylene Glycol Water Based TiO2 Nanofluid in Double Pipe Heat Exchanger with and without Helical Coil Inserts, *International Communications in Heat and Mass Transfer*, *50* (2014), pp. 68-76, DOI: 10.1016/j.icheatmasstransfer.2013.11.002

[31] Kadhim, S. A., *et al.*, Critical Review of the Use of TiO2 Nanofluid as a Heat Transfer Fluid in the Double-Pipe Heat Exchanger, *Journal of Thermal Analysis and Calorimetry*, *150* (2025), 16, pp. 11995-12015, DOI: 10.1007/s10973-025-14531-y

[32] Abbas, A. K., Dhaidan, N. S., Turbulent Forced Convection of Nanofluids Flow in Corrugated Tubes, *IOP Conference Series: Materials Science and Engineering*, *433* (2018), 1, pp. 012054, DOI: 10.1088/1757-899X/433/1/012054

[33] Abdelmagied, M., Investigation of Heat Transfer and Fluid Flow in Annular Curved Tubes in Laminar Flow Using Al2O3–Water Nanofluid, *Discover Applied Sciences*, *6* (2024), 12, pp. 673, DOI: 10.1007/s42452-024-06312-3

[34] Abdelmagied, M., Numerical Analysis on Heat Transfer Enhancement of Al2O3 and CuO-Water Nanofluids in Annular Curved Tubes, *International Journal of Air-Conditioning and Refrigeration*, *33* (2025), 1, pp. 1, DOI: 10.1007/s44189-024-00066-8

[35] Kahalerras, H., Targui, N., Numerical Analysis of Heat Transfer Enhancement in a Double Pipe Heat Exchanger with Porous Fins, *International Journal of Numerical Methods for Heat & Fluid Flow*, *18* (2008), 5, pp. 593-617, DOI: 10.1108/09615530810879738

[36] El Maakoul, A., *et al.*, Performance Enhancement of Finned Annulus Using Surface Interruptions in Double-Pipe Heat Exchangers, *Energy Conversion and Management*, *210* (2020), pp. 112710, DOI: 10.1016/j.enconman.2020.112710

[37] Iqbal, Z., *et al.*, Optimal Fin Shape in Finned Double Pipe with Fully Developed Laminar Flow, *Applied Thermal Engineering*, *51* (2013), 1-2, pp. 1202-1223, DOI: 10.1016/j.applthermaleng.2012.10.036

[38] Iqbal, Z., *et al.*, Fin Design for Conjugate Heat Transfer Optimization in Double Pipe, *International Journal of Thermal Sciences*, *94* (2015), pp. 242-258, DOI: 10.1016/j.ijthermalsci.2015.03.011

[39] Wang, L., *et al.*, Performance of a Double-Tube Heat Exchanger with Staggered Helical Fins, *Chemical Engineering & Technology*, *45* (2022), 5, pp. 953-961, DOI: 10.1002/ceat.202100579

[40] Kiatpachai, P., *et al.*, Air-Side Performance of Embedded and Welded Spiral Fin and Tube Heat Exchangers, *Case Studies in Thermal Engineering*, *30* (2022), pp. 101721, DOI: 10.1016/j.csite.2021.101721

[41] Hosseinkhani, A., *et al.*, Exhaust Gas Heat Recovery Using a Double-Pipe Heat Exchanger with Helical Fins, Considering Gas Radiation Effect: Numerical Investigation, Performance Analysis, and Optimization, *Energy Conversion and Management*, *339* (2025), pp. 119961, DOI: 10.1016/j.enconman.2025.119961

[42] Song, K., *et al.*, Thermal Performance Promotion of a Novel Double-Tube Heat Exchanger by Helical Fin with Perforations, *International Communications in Heat and Mass Transfer*, *150* (2024), pp. 107189, DOI: 10.1016/j.icheatmasstransfer.2023.107189

[43] Hussein, H., *et al.*, Investigation the Influence of the Number and Configuration of Fins on the Hydrothermal Behavior of a Double-Pipe Heat Exchanger, *Journal of Engineering Research*, *13* (2025), 2, pp. 1278-1293, DOI: 10.1016/j.jer.2023.11.006

[44] Yu, C., *et al.*, Enhancing Heat Transfer Efficiency in Corrugated Tube Heat Exchangers: A Comprehensive Approach through Structural Optimization and Field Synergy Analysis, *Heliyon*, *10* (2024), 9, pp. e30113, DOI: 10.1016/j.heliyon.2024.e30113

[45] Dhaidan, N. S., Al-Mousawi, F. N., Thermal-Hydraulic Features of the Turbulent Flow through Ribbed Channels, *Journal of Applied Mechanics and Technical Physics*, *63* (2022), 4, pp. 634-642, DOI: 10.1134/S0021894422040101

[46] Li, C., *et al.*, Dynamic Heat Transfer Characteristics of Ice Storage in Smooth-Tube and Corrugated-Tube Heat Exchangers, *Applied Thermal Engineering*, *223* (2023), pp. 120037, DOI: 10.1016/j.applthermaleng.2023.120037

[47] Shao, C., *et al.*, Novel Extrusion-Expansion Processing for Manufacturing High Performance Micro-Grooved Heat Pipe Heat Exchanger in Low-Grade Waste Heat Recovery Applications, *Journal of Manufacturing Processes*, *156* (2025), pp. 335-348, DOI: 10.1016/j.jmapro.2025.11.053

[48] Duan, Z., *et al.*, Comprehensive Effects of Baffle Configuration on the Performance of Heat Exchanger with Helical Baffles, *Nuclear Engineering and Design*, *300* (2016), pp. 349-357, DOI: 10.1016/j.nucengdes.2016.02.010

[49] Ahirwar, B. K., Kumar, A., An In-Depth Numerical and Experimental Analysis of Wire Coil Inserts: Enhancing Thermal Performance and Fluid Flow Characteristics in Double Pipe Heat Exchangers, *Journal of Thermal Analysis and Calorimetry*, *149* (2024), 23, pp. 14057-14081, DOI: 10.1007/s10973-024-13622-6

[50] Gomaa, A., *et al.*, Investigation of the Hydraulic and Thermal Characteristics of a Double Concentric Tubes with an Inner Twisted Spiral Tube, *Scientific Reports*, *15* (2025), 1, pp. 9301, DOI: 10.1038/s41598-025-92043-3

[51] Liu, J., *et al.*, Numerical Study on a New Spiral Fin Heat Exchanger's Thermal-Hydraulic Performance, *Case Studies in Thermal Engineering*, *61* (2024), pp. 104895, DOI: 10.1016/j.csite.2024.104895

[52] Zhang, L., *et al.*, Heat Transfer Enhancement with Helical Fins and Vortex Generators on Shells at Different Curvatures, *CIESC Journal (Off. J. Chem. Ind. Eng. Soc. China)*, *64* (2013), 9, pp. 3198-3205, DOI: 10.3969/j.issn.0438-1157.2013.09.017

[53] Guo, Z., *et al.*, The Field Synergy (Coordination) Principle and Its Applications in Enhancing Single Phase Convective Heat Transfer, *International Journal of Heat and Mass Transfer*, *48* (2005), 9, pp. 1797-1807, DOI: 10.1016/j.ijheatmasstransfer.2004.11.007

[54] Cao, K., *et al.*, Performance Optimization of Y-Shaped Helical Baffle Heat Exchangers Using Response Surface Methodology, *Applied Thermal Engineering*, (2025), pp. 127002, DOI: 10.1016/j.applthermaleng.2025.127002

[55] Gu, X., *et al.*, Heat Transfer and Flow Resistance Performance of Shutter Baffle Heat Exchanger with Triangle Tube Layout in Shell Side, *Advances in Mechanical Engineering*, *8* (2016), 3, pp. 756504585, DOI: 10.1177/1687814016641015

[56] Tafarroj, M. M., *et al.*, MLP and Optimized FCM-ANFIS Models Proposed for Inlet Turbulent Flow under Ultrasonic Vibration, *Journal of Thermal Analysis and Calorimetry*, *148* (2023), 24, pp. 13995-14009, DOI: 10.1007/s10973-023-12592-5

[57] Esfandyari, M., *et al.*, GMDH and RSM Models for Prediction of Heat Transfer Parameters in an Ultrasonic Vibrating Fin-and-Tube Heat Exchanger, *International Journal of Heat and Fluid Flow*, *114* (2025), pp. 109795, DOI: 10.1016/j.ijheatfluidflow.2025.109795

[58] Khuri, A. I., Mukhopadhyay, S., Response Surface Methodology, *Wiley Interdisciplinary Reviews: Computational Statistics*, *2* (2010), 2, pp. 128-149, DOI: 10.1002/wics.73

[59] El Maakoul, A., *et al.*, Numerical Investigation of Thermohydraulic Performance of Air to Water Double-Pipe Heat Exchanger with Helical Fins, *Applied Thermal Engineering*, *127* (2017), pp. 127-139, DOI: 10.1016/j.applthermaleng.2017.08.024

RECEIVED DATE: 28.11.2025.
DATE OF CORRECTED PAPER: 6.1.2026.
DATE OF ACCEPTED PAPER: 19.2.2026